



Article

Developing a Hybrid Neuro-Fuzzy Method to Predict Carbon Dioxide (CO₂) Permeability in Mixed Matrix Membranes Containing SAPO-34 Zeolite

Ali Hosin Alibak^{1,*}, Seyed Mehdi Alizadeh², Shaghayegh Davodi Monjezi³, As'ad Alizadeh⁴, Falah Alobaid⁵ 
and Babak Aghel^{5,6,*} 

¹ Chemical Engineering Department, Faculty of Engineering, Soran University, Soran 44008, Iraq

² Petroleum Engineering Department, Australian University, West Mishref 11411, Kuwait

³ Department of Environmental Science, Faculty of Natural Resources and Marine Science, Tarbiat Modares University, Nur 46414356, Iran

⁴ Department of Civil Engineering, College of Engineering, Cihan University-Erbil, Erbil 44001, Iraq

⁵ Institut Energiesysteme und Energietechnik, Technische Universität Darmstadt, Otto-Berndt-Straße 2, 64287 Darmstadt, Germany

⁶ Department of Chemical Engineering, Faculty of Energy, Kermanshah University of Technology, Kermanshah 6715685420, Iran

* Correspondence: ali.alibag@soran.edu.iq (A.H.A.); babak.aghel@est.tu-darmstadt.de (B.A.);

Tel.: +49-6151-16-22673 (B.A.); Fax: +49-(0)-6151-16-22690 (B.A.)



Citation: Alibak, A.H.; Alizadeh, S.M.; Davodi Monjezi, S.; Alizadeh, A.; Alobaid, F.; Aghel, B. Developing a Hybrid Neuro-Fuzzy Method to Predict Carbon Dioxide (CO₂) Permeability in Mixed Matrix Membranes Containing SAPO-34 Zeolite. *Membranes* **2022**, *12*, 1147. <https://doi.org/10.3390/membranes12111147>

Academic Editor: Boguslaw Kruczek

Received: 21 October 2022

Accepted: 14 November 2022

Published: 16 November 2022

Publisher's Note: MDPI stays neutral with regard to jurisdictional claims in published maps and institutional affiliations.



Copyright: © 2022 by the authors. Licensee MDPI, Basel, Switzerland. This article is an open access article distributed under the terms and conditions of the Creative Commons Attribution (CC BY) license (<https://creativecommons.org/licenses/by/4.0/>).

Abstract: This study compares the predictive performance of different classes of adaptive neuro-fuzzy inference systems (ANFIS) in predicting the permeability of carbon dioxide (CO₂) in mixed matrix membrane (MMM) containing the SAPO-34 zeolite. The hybrid neuro-fuzzy technique uses the MMM chemistry, pressure, and temperature to estimate CO₂ permeability. Indeed, grid partitioning (GP), fuzzy C-means (FCM), and subtractive clustering (SC) strategies are used to divide the input space of ANFIS. Statistical analyses compare the performance of these strategies, and the spider graph technique selects the best one. As a result of the prediction of more than 100 experimental samples, the ANFIS with the subtractive clustering method shows better accuracy than the other classes. The hybrid optimization algorithm and cluster radius = 0.55 are the best hyperparameters of this ANFIS model. This neuro-fuzzy model predicts the experimental database with an absolute average relative deviation (AARD) of less than 3% and a correlation of determination higher than 0.995. Such an intelligent model is not only straightforward but also helps to find the best MMM chemistry and operating conditions to maximize CO₂ separation.

Keywords: mixed matrix membrane; SAPO-34 zeolite; carbon dioxide separation; theoretical analysis; adaptive neuro-fuzzy inference system (ANFIS)

1. Introduction

Environmental pollution [1], global warming [2], and climate change [3], are likely the most interconnected problematic issues in recent decades. Carbon dioxide (CO₂) as a greenhouse gas is undeniably a key factor in creating these undesirable environmental phenomena [4]. Therefore, separating and recycling CO₂ from the gaseous streams released to the atmosphere seems essential. In addition, separating the CO₂ impurity of the natural gas is significant to improve the heating value and avoid corrosion in transmission pipelines and processing equipment. Absorption [5], adsorption [6,7], cryogenic process [8,9], and membrane-based [10] operations are conventionally applied to separate CO₂ molecules from either waste or raw gaseous stream. In addition, the recovered carbon dioxide can be then used for the separation of heavy metal pollutants [11].

The membrane-based technologies, which are low cost, highly flexible, easy to operate, energy saving, and environmentally friendly [12], have seen a growing interest in the field

of CO₂ capture. Due to their suitable mechanical characteristics, the polymeric membranes work better in high-pressure and temperature situations. Researchers have continuously attempted to fabricate materials that fulfill the trade-off between gas selectivity and permeability and overcome the “Robeson upper bond” curve in polymeric membranes. To do so, attention has been concentrated on the inclusion of inorganic solid materials in the polymer membrane structure [13].

The mixed matrix membranes (MMM), which combine a polymer as the continuous phase and inorganic filler as the dispersed phase, have been suggested to resolve these limitations [14]. This special class of membranes shows better gas separation performance than both polymer and inorganic fillers [15]. Activated carbon [16], nano-fibers [17], nanoparticles [18], metal-[19] and [20] covalent organic frameworks, and zeolites [21], have been successfully dispersed in polymers' structure to fabricate MMMs.

Due to high pore volume, uniform pore size distribution, and appropriate chemical/thermal stability, zeolites [22] and their inclusion in a matrix [23] are often used for the CO₂ separation. The SAPO-34 zeolite, with excellent CO₂ adsorption affinity, has achieved great popularity in synthesizing mixed matrix membranes [23]. These investigations have mainly measured the CO₂ permeability in mixed matrix membranes experimentally. The permeability measurements have been considered as a function of polymer type, SAPO-34 dosage, pressure, and temperature.

Despite a relatively extensive experimental analysis of CO₂ permeability in MMMs, there is no systematic strategy to predict this key variable. Therefore, the current research uses a hybrid neuro-fuzzy modeling approach to predict CO₂ permeability in MMMs containing SAPO-34 as a function of polymer type, SAPO-34 dosage, pressure, and temperature. A hybrid optimization algorithm and sensitivity analysis determine this model's adjustable coefficient and its hyperparameters, respectively. The proposed model in this study can help construct the MMM-based CO₂ removal facility by providing accurate predictions for CO₂ permeability as a function of MMM chemistry and operating conditions.

2. Literature Data

Different MMMs have already been fabricated by combining SAPO-34 zeolite and Matrimid-5218 [24], Pebax-1657 [25], polyethersulfone [26,27], polyurethane [28], polysulfone [29], and Pebax-1074 [30] polymers for the purpose of CO₂ removal. The literature measured the CO₂ permeability in these MMMs as a function of SAPO-34 dosage, temperature, and pressure. Table 1 presents numerical values of the statistical information (minimum, maximum, average, and standard deviation) of these experimental measurements, and Figure 1 illustrates their graphical version using the box plot. It can be seen that the collected experimental databank covers SAPO-34 dosage, temperature, and pressure ranges of 0–50 wt.%, 267–394 K, and 0.1–3 MPa. In this condition, the CO₂ permeability varies from 0.2–337 barrer.

Table 1. Statistical information of the collected experimental databank [24–30].

Variable	Min	Max	Average	Standard Deviation
SAPO-34 dosage (wt%)	0	50	13.70	11.75
Temperature (K)	267	394	303.75	16.57
Pressure (MPa)	0.1	3	0.985	0.614
CO ₂ perm (barrer)	0.20	337	107.88	83.64

In addition to these statistical and graphical presentations of the experimental measurements, the Supplementary Material reports all their information.

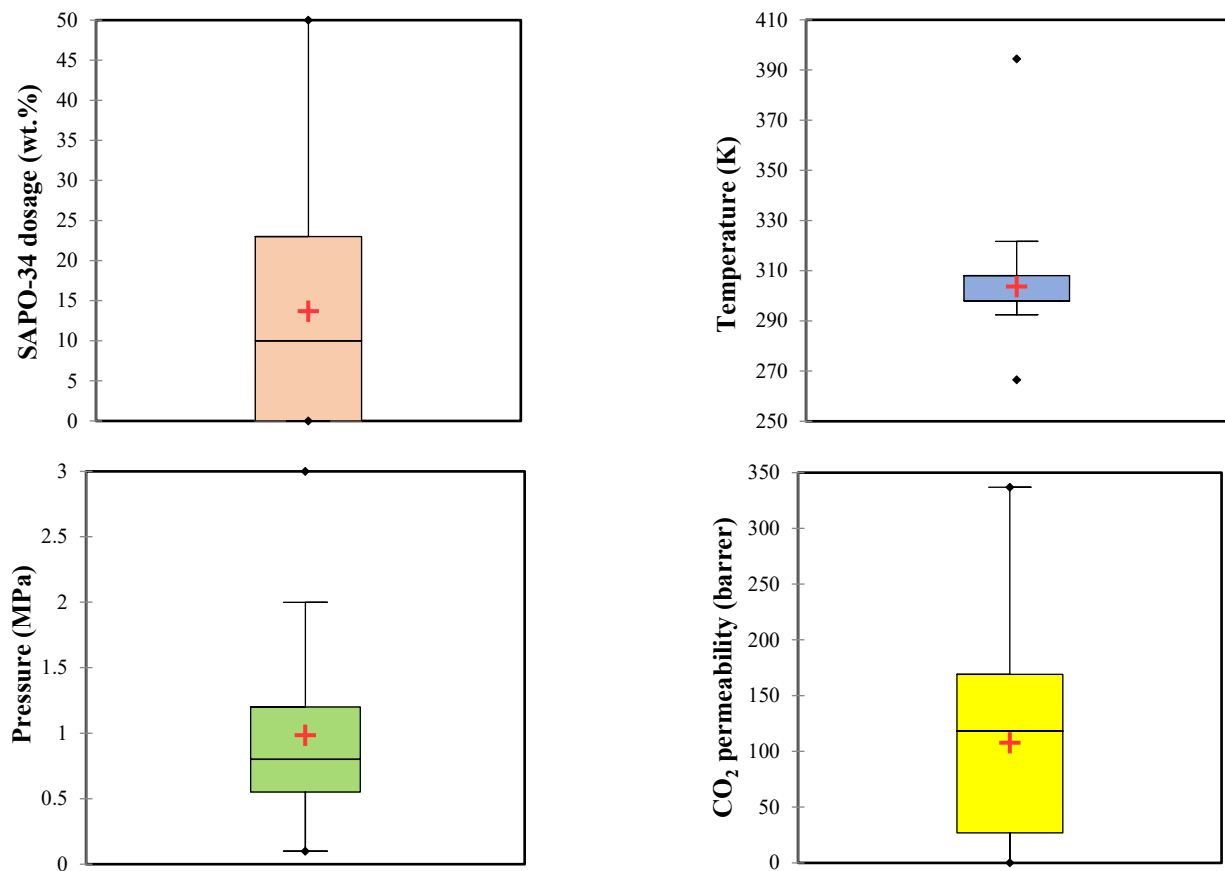


Figure 1. Box plot presentation of statistical information of the collected experimental databank.

3. ANFIS Description

3.1. ANFIS Structure

The function approximation [31] and classification [32] are the problems that can be easily handled by the machine learning tools. Therefore, this study aims to efficiently tune the adaptive neuro-fuzzy inference system topology to enhance the prediction accuracy of CO₂ permeability in different MMMs in a broad range of operating conditions. Consequently, it seems necessary to briefly describe the working procedure of this intelligent estimation machine.

The ANFIS is a powerful modeling tool that simultaneously utilizes the inference property of fuzzy logic and the learning capabilities of artificial neural networks. Consider a multiple-input and single-output (MISO) regression problem, such as $F(X, Y)$. A Takagi–Sugeno system with five interconnected successive layers (i.e., fuzzification, interference, normalization, interpolation, and target computation) and the following fuzzy if–then rules, namely Equations (1) and (2) [33], can be constructed to model this problem.

$$\text{Rule 1: If } X \text{ is } A_1 \text{ and } Y \text{ is } B_1, \text{ then } F_1 = C_1 \times X + D_1 \times Y + E_1 \quad (1)$$

$$\text{Rule 2: If } X \text{ is } A_2 \text{ and } Y \text{ is } B_2, \text{ then } F_2 = C_2 \times X + D_2 \times Y + E_2 \quad (2)$$

Here, $A_1, A_2, B_1,$ and B_2 are the premise parameters. On the other hand, the adjustable consequence parameters are shown by $C_1, C_2, D_1, D_2, E_1,$ and E_2 .

The first layer assigns a membership function (η) to each node j and calculates the output signals (O_j^1) based on Equations (3) and (4) [34].

$$O_j^1 = \eta_{A_j}(X) \quad j = 1, 2 \quad (3)$$

$$O_j^1 = \eta_{B_{j-2}}(Y) \quad j = 3, 4 \tag{4}$$

The output of the second layer (O_j^2) is the product of all the incoming signals [35].

$$O_j^2 = \eta_{A_j}(X) \eta_{B_j}(Y) = \omega_j \quad j = 1, 2 \tag{5}$$

The outputs of the third layer (O_j^3) compute by normalizing the entry signals, as in Equation (6) [36].

$$O_j^3 = \bar{\omega}_j = \omega_j / (\omega_1 + \omega_2) \quad j = 1, 2 \tag{6}$$

Then, Equation (7) calculates the outputs of the fourth layer (O_j^4) [37].

$$O_j^4 = \bar{\omega}_j F_j = \bar{\omega}_j (C_j X + D_j Y + E_j) \quad j = 1, 2 \tag{7}$$

Finally, the ANFIS prediction for the target (O^{ANFIS}) can be achieved by applying Equation (8) [38].

$$O^{ANFIS} = \sum_{j=1}^2 \bar{\omega}_j F_j \tag{8}$$

3.2. Input Space Partitioning Strategies

The literature declares that the fuzzification strategy (the first layer of ANFIS) significantly impacts the accuracy of simulating a given problem [39]. Generally, there are three well-known methods to divide the input space, i.e., grid partitioning (GP), fuzzy C-means (FCM), and subtractive clustering (SC). Although Yeom and Kwak comprehensively described GP, FCM, and SC and highlighted their weaknesses and strengths [33], the following subsections briefly explain these partitioning strategies.

3.2.1. Grid Partitioning

Grid partitioning is a method that breaks down input space into a non-overlapping grid-like structure. This method is suitable for a problem with a small number of independent variables in low-dimensional input space. For instance, 1024 unique areas and a rule for each area (i.e., 1024 rules) have been provided by the GP method with two membership functions for a problem with 10 independent variables [33]. Hence, the GP is a complicated strategy to divide the input space of a high-dimensional problem (high number of the independent variable of observations).

3.2.2. Fuzzy c-Means Clustering

The FCM separates the input space and places them in different fuzzy clusters with a specific radius. An optimization method that minimizes the observed non-similarity determines these properties. The user specifies the number of fuzzy rules by setting the number of clusters.

3.2.3. Subtractive Clustering

The SC is a scenario to break down the input space into several specific clusters by performing a multi-dimensional analysis. This strategy automatically divides the input space into an appropriate number of clusters utilizing a user-entered value for the cluster radius. The SC generates a high number of small-sized clusters when a small cluster radius is entered, and vice versa.

3.3. Training Algorithm

Traditionally the backpropagation or hybrid training algorithm is applied to determine adjustable parameters of membership functions during the training step of the ANFIS. The backpropagation method continuously updates the adjustable parameters of the ANFIS to minimize the deviation between actual and predicted values of a dependent variable. Indeed, the observed deviation propagates backward through the ANFIS structure, and its

parameters adjust by several iterations. On the other hand, the hybrid method combines the least-squares and backpropagation algorithms to tune ANFIS parameters efficiently. To enhance the performance of the training phase, as well as to avoid errors related to the different ranges of variables, the experimental data are needed to normalize between 0 and 1 [40,41].

4. Results and Discussion

The most appropriate structural features for three well-known ANFIS types have been determined in this section. Four statistical uncertainty criteria, i.e., absolute average relative deviation (AARD%), mean squared error (MSE), root mean squared error (RMSE), and correlation of determination (R), are often applied to perform such comparison [42,43]. Equations (9)–(12) express that these uncertainty criteria quantize the compatibility between laboratory-measured CO₂ permeability in MMMs ($\lambda_{CO_2}^{lab}$) and its counterpart simulation by the ANFIS models ($\lambda_{CO_2}^{sim}$).

$$R = \sqrt{1 - \left\{ \frac{\sum_{i=1}^n (\lambda_{CO_2}^{lab} - \lambda_{CO_2}^{sim})^2}{\sum_{i=1}^n (\lambda_{CO_2}^{lab} - \overline{\lambda_{CO_2}^{lab}})^2} \right\}} \tag{9}$$

$$AARD\% = (100/n) \times \sum_{i=1}^n \left(\left| \lambda_{CO_2}^{lab} - \lambda_{CO_2}^{sim} \right| / \lambda_{CO_2}^{lab} \right)_i \tag{10}$$

$$MSE = (1/n) \times \sum_{i=1}^n \left(\lambda_{CO_2}^{lab} - \lambda_{CO_2}^{sim} \right)_i^2 \tag{11}$$

$$RMSE = \sqrt{(1/n) \times \sum_{i=1}^n \left(\lambda_{CO_2}^{lab} - \lambda_{CO_2}^{sim} \right)_i^2} \tag{12}$$

Then, the most accurate neuro-fuzzy model is identified by the spider plot analysis. Different graphical analyses then deeply assess the performance of the selected ANFIS model. Finally, the effect of filler dosage, pressure, and temperature on the CO₂ permeability in the MMM is investigated.

4.1. Developing ANFIS Models

As noted, GP, FCM, and SC strategies have been used to divide the input space of ANFIS. Therefore, it is possible to develop and compare three ANFIS types, i.e., ANFIS-GP, ANFIS-FCM, and ANFIS-SC. Table 2 reports the investigated ranges of structural features for each ANFIS type and the selected one by statistical analyses. This table states that the ANFIS-GP and ANFIS-FCM should construct with two and eleven clusters, respectively, while the cluster radius of the ANFIS-SC model should fix at 0.55. The hybrid algorithm is better at performing the training step of all three ANFIS types than the backpropagation.

Table 2. The checked and selected structural features of different ANFIS types.

Model	Checked Features	The Best Features
ANFIS-GP	Cluster number: 2:1:5 Optimization algorithm: backpropagation and hybrid	Two clusters Hybrid
ANFIS-FCM	Cluster number: 2:1:12 Optimization algorithm: backpropagation and hybrid	Eleven clusters Hybrid
ANFIS-SC	Cluster radius: 0.1:0.05:1 Optimization algorithm: backpropagation and hybrid	Cluster radius = 0.55 Hybrid

Table 3 utilizes AARD%, MSE, RMSE, and R-value to measure/compare the accuracy of the selected ANFIS models. The accuracy has been separately monitored for the training,

testing, and overall databank. Although all these accuracies are valuable from the modeling point of view, the performance of the ANFIS-FCM and ANFIS-SC is far better than the ANFIS-GP. The next sections apply the spider plot to select the most suitable ANFIS type to estimate CO₂ permeability in the mixed matrix membranes containing SAPO-34 zeolite.

Table 3. Performance analysis of the selected ANFIS models by four statistical indexes.

Model	Database	AARD%	MSE	RMSE	R
ANFIS-GP	Training	4.03	25.54	5.05	0.9981
	Testing	18.91	77.05	8.78	0.9958
	Overall	6.19	33.05	5.75	0.9976
ANFIS-FCM	Training	3.02	40.09	6.33	0.9972
	Testing	8.78	299.98	17.32	0.9823
	Overall	3.86	77.94	8.83	0.9946
ANFIS-SC	Training	1.85	5.59	2.37	0.9996
	Testing	4.38	70.70	8.41	0.9952
	Overall	2.22	15.08	3.88	0.9989

4.2. Choosing the Best ANFIS Type

Before performing the model selection analysis, it is better to highlight that a model with a low AARD%, MSE, RMSE, and close R-value to one is preferable from a modeling point of view. The spider plot is a graphical method to compare the statistical indexes provided by ANFIS-GP, ANFIS-FCM, and ANFIS-SC at a glance. In other words, the spider analysis presents the reported statistical values in Table 3 in a multi-dimensional graph.

The results of comparing the performance of ANFIS-GP, ANFIS-FCM, and ANFIS-SC in the training and testing groups and the whole database have been shown in Figure 2a–c, respectively. These spider graphs can be easily analyzed to compare the provided AARD%, MSE, RMSE, and R indexes by different ANFIS types.

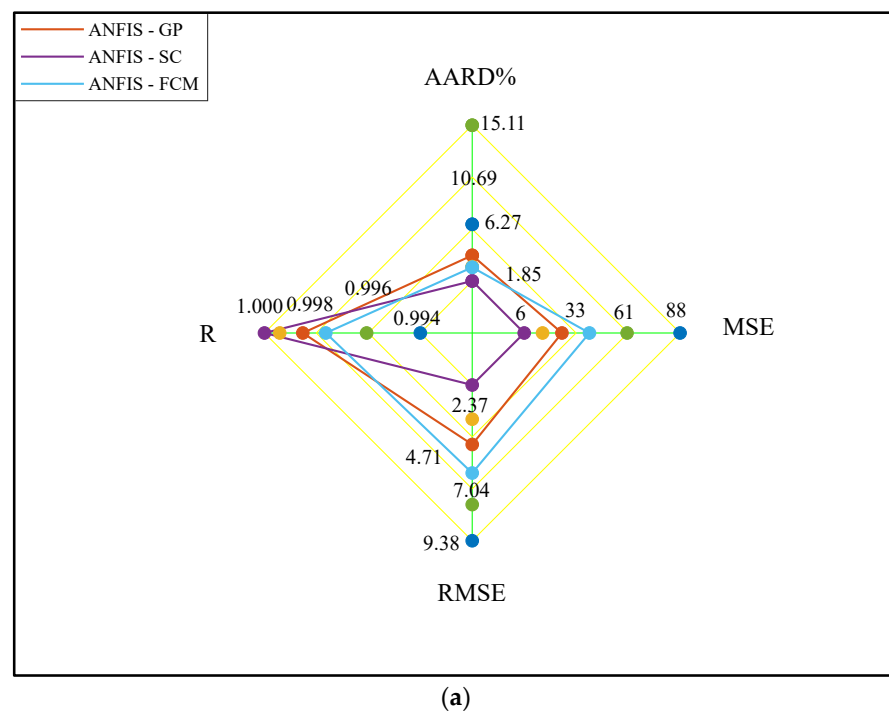
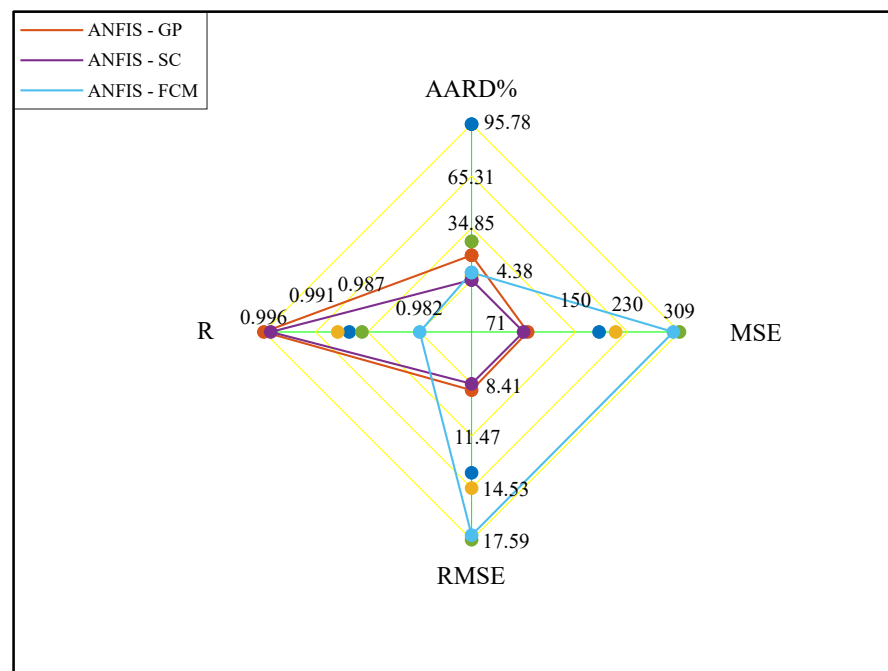
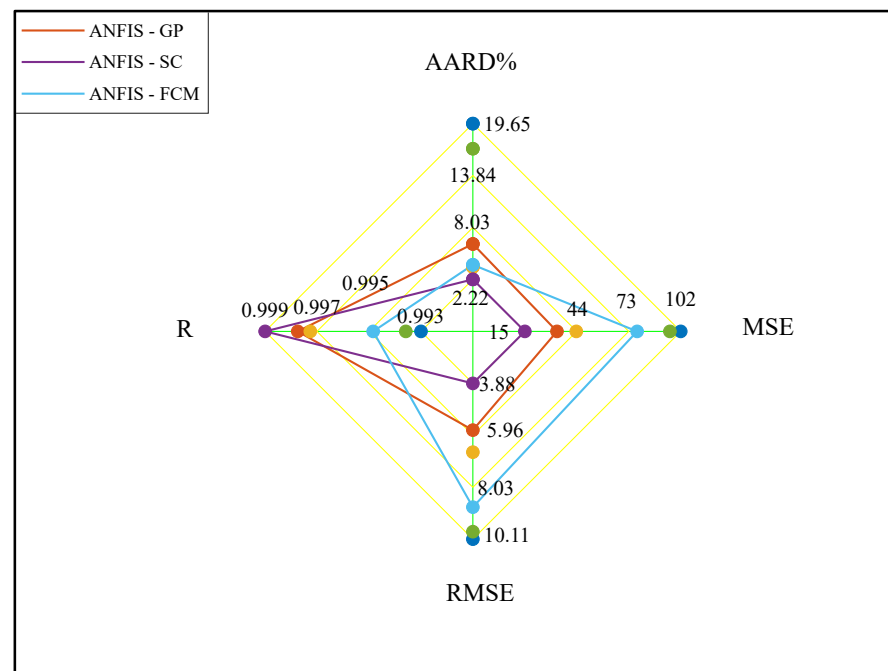


Figure 2. Cont.



(b)



(c)

Figure 2. Spider plot for comparing the ANFIS models’ performance in the (a) training, (b) testing, and (c) all of the database.

The spider graph analyses (Figure 2a,b) indicated that the ANFIS-SC performs better when predicting the training and testing datasets of CO₂ permeability in the MMMs. Since the overall databank combines the training and testing groups, it is obvious that the ANFIS-SC accuracy is also better than the two other models (Figure 2c).

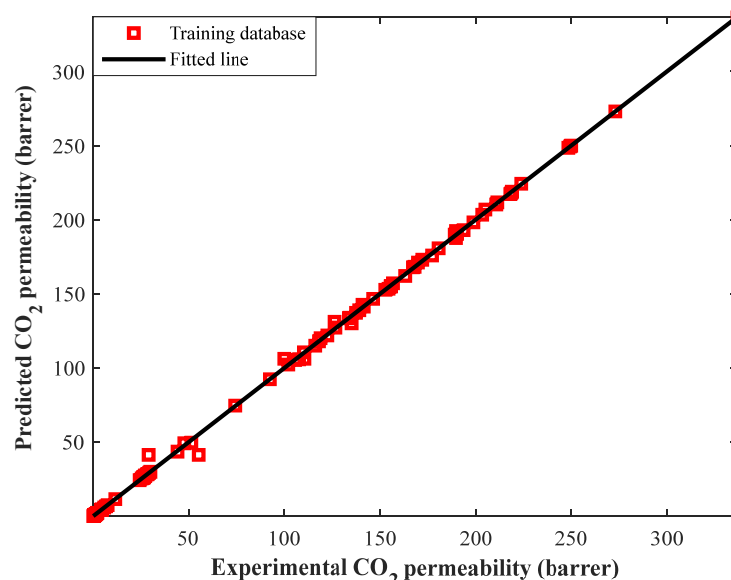
4.3. Evaluating the Performance of the Selected ANFIS Model

This section comprehensively evaluates the reliability of ANFIS-SC performance in predicting CO₂ permeability in MMMs by combining statistical and visual inspections. The

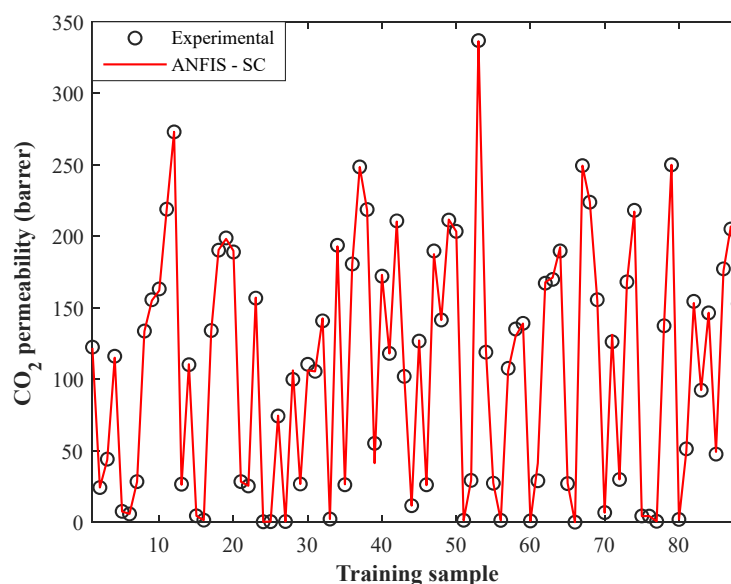
performance assessment has been separately performed for the training and testing groups and their combination (i.e., overall databank).

4.3.1. Training Step

The correlation between experimental CO₂ permeabilities in MMMs and their corresponding predictions by ANFIS-SC in the training step has been plotted in Figure 3a. Since all square symbols are gathered around the diagonal line, it can be claimed that the ANFIS-SC model accurately predicts the training datasets.



(a)



(b)

Figure 3. (a) Cross-plot of ANFIS-SC predictions versus experimental CO₂ permeabilities in the training step. (b) Experimental CO₂ permeabilities and their related ANFIS-SC predictions in the training step.

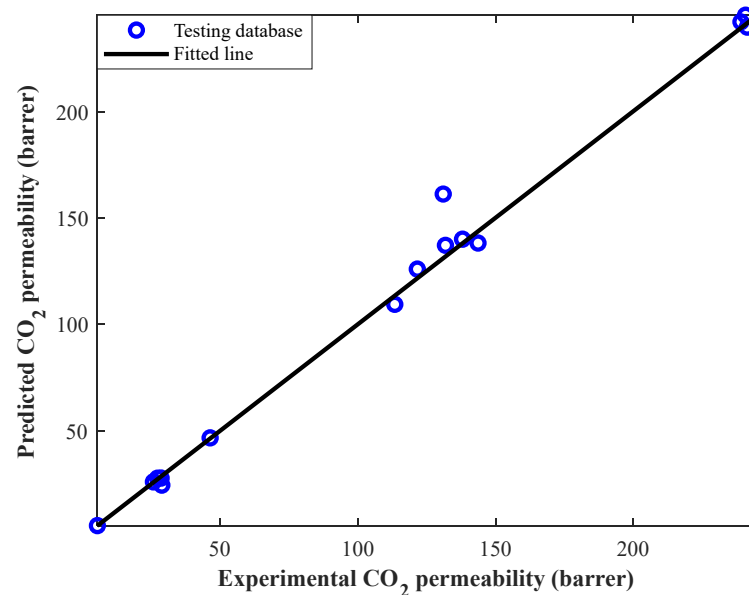
Visually comparing the actual and predicted values of a dependent variable is a well-known method to check the accuracy of a model [44]. Thus, numerical values of the CO₂ permeability in MMMs in the training step, as well as their associated ANFIS-SC

predictions, have been illustrated in Figure 3b. This figure approves excellent compatibility between laboratory-measured and ANFIS-SC predictions in the training phase.

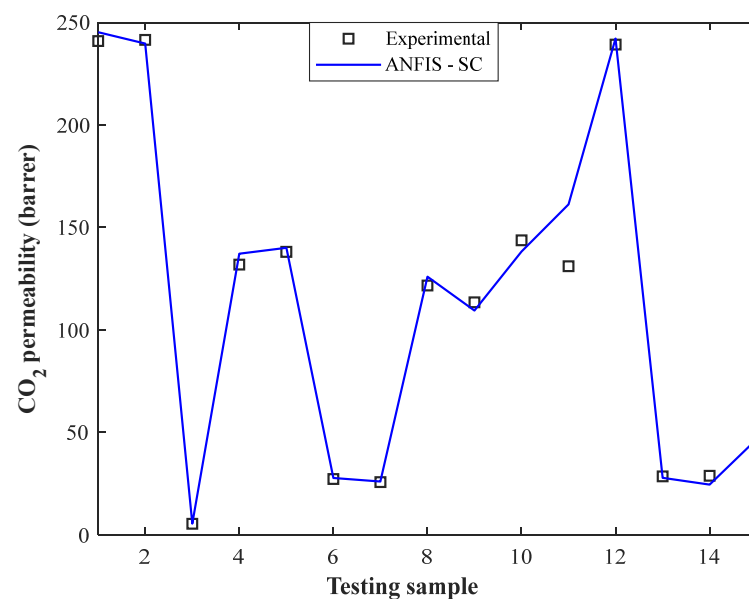
Indeed, the ANFIS-SC predicts 88 actual CO₂ permeabilities in MMMs with the AARD = 1.85%, MSE = 5.59, RMSE = 2.37, and R = 0.9996.

4.3.2. Testing Step

This analysis correlates the experimental CO₂ permeabilities in MMMs and their related ANFIS-SC predictions in the testing step (Figure 4a). It can be seen that the model predictions have been precisely mapped on the experimentally measured data. Indeed, the ANFIS-SC predicts 15 actual CO₂ permeabilities in MMMs with the AARD = 4.38%, MSE = 70.70, RMSE = 8.41, and R = 0.9952.



(a)



(b)

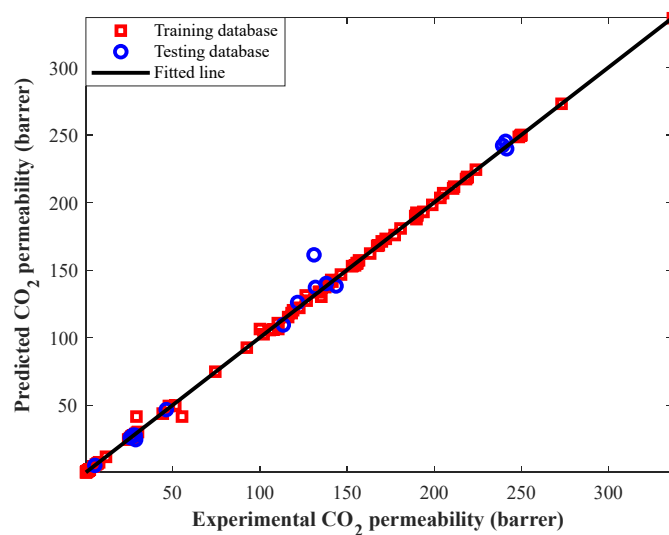
Figure 4. (a) Cross-plot of ANFIS-SC predictions versus experimental CO₂ permeabilities in the testing step. (b) Experimental CO₂ permeabilities and their related ANFIS-SC predictions in the testing step.

Figure 4b also presents the numerical values of actual and estimated CO₂ permeability in MMMs in the testing step of the ANFIS-SC. Since the model has seen none of these samples before, its excellent performance for simulating CO₂ separation by the MMM can be observed. Indeed, the ANFIS-SC accurately predicts all unknown CO₂ permeability in MMMs at the testing stage except for one sample.

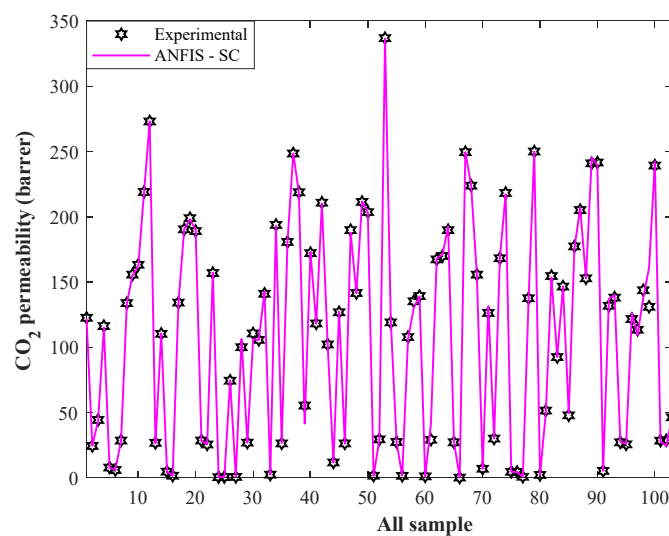
4.3.3. All Experimental Data

This section analyzes the ANFIS-SC performance in predicting the overall databank of CO₂ permeability in mixed matrix membranes. Since the overall databank is a combination of the training and testing groups, it is expected that the ANFIS-SC model will also have an excellent performance in this analysis.

The experimental and simulated CO₂ permeabilities in MMMs for training and testing groups (overall databank) have been presented in Figure 5a. This figure confirms a remarkable agreement between the laboratory-measured and simulated values. Indeed, the ANFIS-SC predicts 103 actual CO₂ permeabilities in MMMs with the AARD = 2.22%, MSE = 15.08, RMSE = 3.88, and R = 0.9989.



(a)



(b)

Figure 5. (a) Correlation between experimental and predicted CO₂ permeabilities for the whole of experimental databank. (b) Experimental CO₂ permeabilities and their associated ANFIS-SC predictions for the combination of training and testing datasets.

Figure 5b also presents the ANFIS-SC prediction for each experimental measurement separately. The outstanding performance of this model in simulating CO₂ separation by the mixed matrix membranes can be justified by this figure.

4.4. Investigating the Effect of SAPO-34 Dosage, Pressure, and Temperature

The effect of filler dosage on the isothermal CO₂ permeability (298 K) in Pebax-1074/SAPO-34 MMMs at six pressure levels has been illustrated in Figure 6. This figure displays experimental CO₂ permeability profiles and their corresponding simulations by the ANFIS-SC model. The designed model not only correctly anticipates the trend of experimental profiles but also accurately estimates all individual data points. Actually, the proposed neuro-fuzzy model easily identifies the effect of pressure and filler dosage on the CO₂ permeability in Pebax-1074/SAPO-34 mixed matrix membranes.

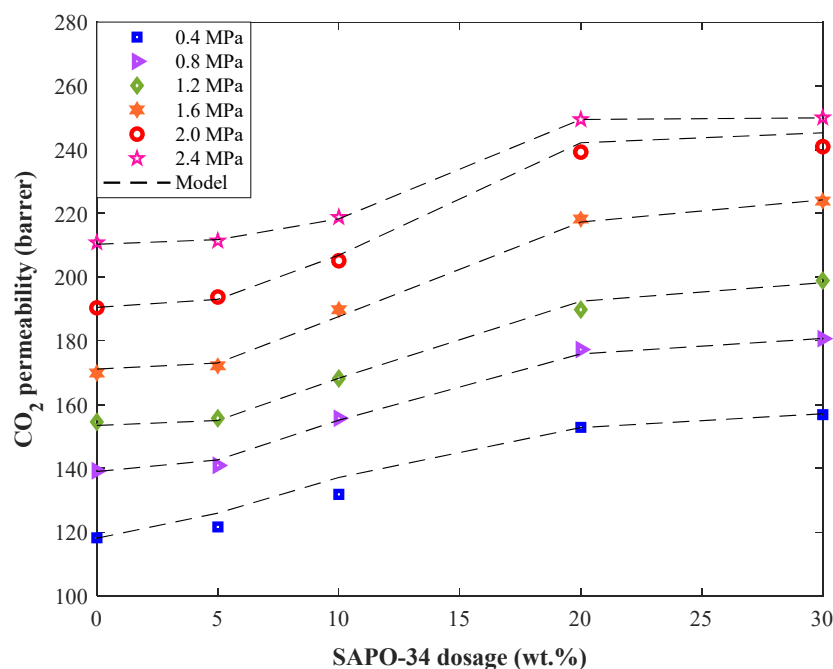


Figure 6. Monitoring the effect of SAPO-34 dosage and pressure on the CO₂ permeability in Pebax-1074-based MMM (298 K).

This figure also shows that the CO₂ permeability in the Pebax-1074/SAPO-34 is enhanced by increasing either pressure or filler dosage. The maximum CO₂ permeability of 250 barrer is achieved at the maximum pressure and SAPO-34 dosage of 2.4 MPa and 30 wt.%, respectively.

The simulation and experimental profiles for the isobaric CO₂ permeability (0.7 MPa) in Pebax-1657/SAPO-34 MMMs as a function of temperature have been shown in Figure 7. This figure can readily demonstrate the outstanding compatibility between the actual and simulation profiles. This analysis also indicates that the CO₂ permeability in the pure Pebax-1657 may be increased by more than 40 barrers by adding 30 wt.% of SAPO-34 zeolite. In addition, the increasing effect of temperature on the CO₂ permeability in both pure Pebax-1657 and Pebax-1657/SAPO-34 MMM is observable in Figure 7.

4.5. Identifying Undesirable Outliers

The leverage method provides a practical ground to identify undesirable outliers in an experimental database [45]. Figure 8 shows that a small number of experimental data (i.e., 4 samples) are undesirable outliers. Since almost all the samples are valid, the undesirable effect of outliers on the model prediction can be ignored.

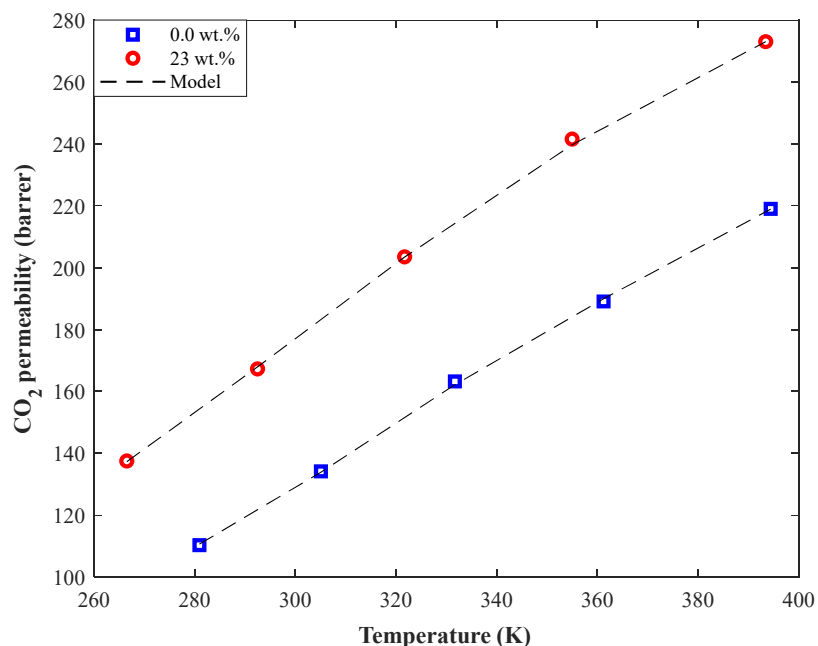


Figure 7. The effect of temperature on the CO₂ permeability in pure Pebax-1657 and Pebax-1657/SAPO-34 MMM (0.7 MPa).

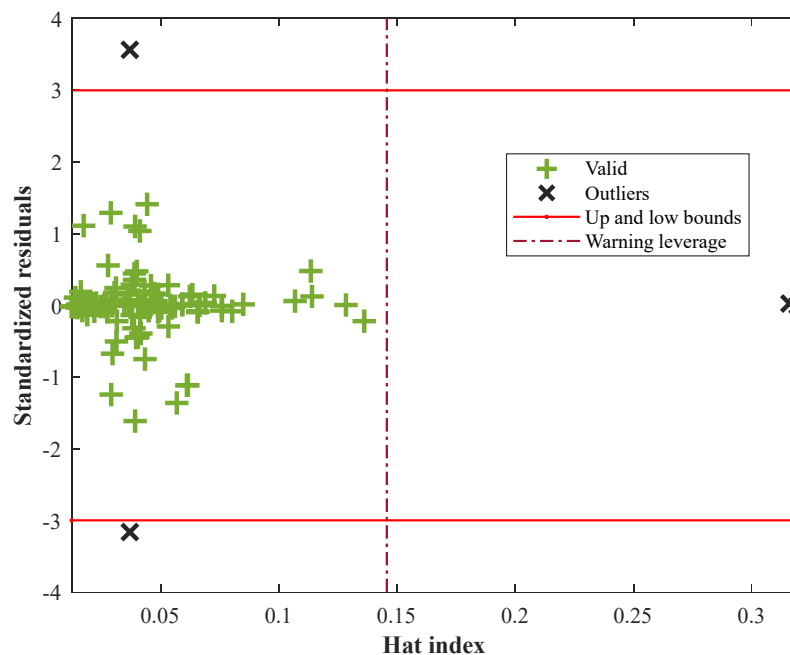


Figure 8. Employing the leverage method to identify undesirable outliers.

5. Conclusions

The current research combined the statistical and graphical analyses to compare the performance of three neuro-fuzzy types (i.e., ANFIS-GP, ANFIS-FCM, and ANFIS-SC) in predicting the CO₂ separation ability of six different mixed matrix membranes containing SAPO-34 zeolite as a filler. The ANFIS-SC trained by the hybrid algorithm has been identified as the most reliable model for estimating the considered matter. This model predicted 103 experimentally measured CO₂ permeability values in a wide range of membrane compositions and operating conditions with the AARD = 2.22%, MSE = 15.08, RMSE = 3.88, and R = 0.9989. In addition, the visual inspections have also justified the

outstanding ability of the proposed neuro-fuzzy model in simulating CO₂ separation by mixed matrix membranes. The simulation and experimental results showed that the CO₂ permeability in all investigated MMMs can be increased by increasing the SAPO-34 dosage, pressure, and temperature. The proposed intelligent model in this study can quickly determine the membrane composition and operating conditions so that the CO₂ permeability is maximized.

Supplementary Materials: The following supporting information can be downloaded at: <https://www.mdpi.com/article/10.3390/membranes12111147/s1>. Table S1: The analyzed experimental data.

Author Contributions: A.H.A.: Writing—original draft, Writing—review & editing, Conceptualization, Methodology, Resources; S.M.A.: Writing—original draft, Writing—review & editing, Investigation, Conceptualization; S.D.M.: Writing—original draft, Writing—review & editing, Resources, Investigation; A.A.: Writing—original draft, Writing—review & editing, Validation; F.A.: Resources, Supervision; B.A.: Writing—Review. All authors have read and agreed to the published version of the manuscript.

Funding: This research received no external funding.

Institutional Review Board Statement: Not applicable.

Informed Consent Statement: Not applicable.

Data Availability Statement: The analyzed experimental data in this research is available in the Supplementary Material.

Acknowledgments: We acknowledge support by the Deutsche Forschungsgemeinschaft (DFG—German Research Foundation) and the Open Access Publishing Fund of Technical University of Darmstadt.

Conflicts of Interest: The authors declare no conflict of interest.

References

1. Liang, L.; Wang, Z.; Li, J. The effect of urbanization on environmental pollution in rapidly developing urban agglomerations. *J. Clean. Prod.* **2019**, *237*, 117649. [CrossRef]
2. Zandalinas, S.I.; Fritschi, F.B.; Mittler, R. Global warming, climate change, and environmental pollution: Recipe for a multifactorial stress combination disaster. *Trends Plant Sci.* **2021**, *26*, 588–599. [CrossRef] [PubMed]
3. Goglio, P.; Williams, A.G.; Balta-Ozkan, N.; Harris, N.R.P.; Williamson, P.; Huisingh, D.; Zhang, Z.; Tavoni, M. Advances and challenges of life cycle assessment (LCA) of greenhouse gas removal technologies to fight climate changes. *J. Clean. Prod.* **2020**, *244*, 118896. [CrossRef]
4. Zhou, Z.; Davoudi, E.; Vaferi, B. Monitoring the effect of surface functionalization on the CO₂ capture by graphene oxide/methyl diethanolamine nanofluids. *J. Environ. Chem. Eng.* **2021**, *9*, 106202. [CrossRef]
5. Aghel, B.; Heidaryan, E.; Sahraie, S.; Mir, S. Application of the microchannel reactor to carbon dioxide absorption. *J. Clean. Prod.* **2019**, *231*, 723–732. [CrossRef]
6. Karimi, M.; Rodrigues, A.E.; Silva, J.A.C. Designing a simple volumetric apparatus for measuring gas adsorption equilibria and kinetics of sorption. Application and validation for CO₂, CH₄ and N₂ adsorption in binder-free beads of 4A zeolite. *Chem. Eng. J.* **2021**, *425*, 130538. [CrossRef]
7. Qu, M.; Chen, Z.; Sun, Z.; Zhou, D.; Xu, W.; Tang, H.; Gu, H.; Liang, T.; Hu, P.; Li, G.; et al. Rational design of asymmetric atomic Ni-P1N₃ active sites for promoting electrochemical CO₂ reduction. *Nano Res.* **2022**, 1–7. [CrossRef]
8. Tengku Hassan, T.N.A.; Shariff, A.M.; Mohd Pauzi, M.M.; Khidzir, M.S.; Surmi, A. Insights on Cryogenic Distillation Technology for Simultaneous CO₂ and H₂S Removal for Sour Gas Fields. *Molecules* **2022**, *27*, 1424. [CrossRef]
9. Xu, W.; LI, C.H.; Zhang, Y.; Ali, H.M.; Sharma, S.; Li, R.; Yang, M.; Gao, T.; Liu, M.; Wang, X.; et al. Electrostatic atomization minimum quantity lubrication machining: From mechanism to application. *Int. J. Extrem. Manuf.* **2022**, *4*, 042003. [CrossRef]
10. Endeward, V.; Arias-Hidalgo, M.; Al-Samir, S.; Gros, G. CO₂ permeability of biological membranes and role of CO₂ channels. *Membranes* **2017**, *7*, 61. [CrossRef]
11. Mo, X.; Liu, X.; Chen, J.; Zhu, S.; Xu, W.; Tan, K.; Wang, Q.; Lin, Z.; Liu, W. Separation of lattice-incorporated Cr(vi) from calcium carbonate by converting microcrystals into nanocrystals via the carbonation pathway based on the density functional theory study of incorporation energy. *Environ. Sci. Nano* **2022**, *9*, 1617–1626. [CrossRef]
12. Wu, R.; Tan, Y.; Meng, F.; Zhang, Y.; Huang, Y.-X. PVDF/MAF-4 composite membrane for high flux and scaling-resistant membrane distillation. *Desalination* **2022**, *540*, 116013. [CrossRef]

13. Aroon, M.A.; Ismail, A.F.; Matsuura, T.; Montazer-Rahmati, M.M. Performance studies of mixed matrix membranes for gas separation: A review. *Sep. Purif. Technol.* **2010**, *75*, 229–242. [[CrossRef](#)]
14. Casado-Coterillo, C. Mixed matrix membranes. *Membranes* **2019**, *9*, 149. [[CrossRef](#)] [[PubMed](#)]
15. Junaidi, M.U.M.; Khoo, C.P.; Leo, C.P.; Ahmad, A.L. The effects of solvents on the modification of SAPO-34 zeolite using 3-aminopropyl trimethoxy silane for the preparation of asymmetric polysulfone mixed matrix membrane in the application of CO₂ separation. *Microporous Mesoporous Mater.* **2014**, *192*, 52–59. [[CrossRef](#)]
16. Weigelt, F.; Georgopoulos, P.; Shishatskiy, S.; Filiz, V.; Brinkmann, T.; Abetz, V. Development and characterization of defect-free Matrimid[®] mixed-matrix membranes containing activated carbon particles for gas separation. *Polymers* **2018**, *10*, 51. [[CrossRef](#)] [[PubMed](#)]
17. Kiadehi, A.D.; Rahimpour, A.; Jahanshahi, M.; Ghoreyshi, A.A. Novel carbon nano-fibers (CNF)/polysulfone (PSf) mixed matrix membranes for gas separation. *J. Ind. Eng. Chem.* **2015**, *22*, 199–207. [[CrossRef](#)]
18. Soltani, B.; Asghari, M. Effects of ZnO nanoparticle on the gas separation performance of polyurethane mixed matrix membrane. *Membranes* **2017**, *7*, 43. [[CrossRef](#)]
19. Chuah, C.Y.; Samarasinghe, S.; Li, W.; Goh, K.; Bae, T.-H. Leveraging nanocrystal HKUST-1 in mixed-matrix membranes for ethylene/ethane separation. *Membranes* **2020**, *10*, 74. [[CrossRef](#)]
20. Duan, K.; Wang, J.; Zhang, Y.; Liu, J. Covalent organic frameworks (COFs) functionalized mixed matrix membrane for effective CO₂/N₂ separation. *J. Memb. Sci.* **2019**, *572*, 588–595. [[CrossRef](#)]
21. Bastani, D.; Esmaili, N.; Asadollahi, M. Polymeric mixed matrix membranes containing zeolites as a filler for gas separation applications: A review. *J. Ind. Eng. Chem.* **2013**, *19*, 375–393. [[CrossRef](#)]
22. Henrique, A.; Karimi, M.; Silva, J.A.C.; Rodrigues, A.E. Analyses of Adsorption Behavior of CO₂, CH₄, and N₂ on Different Types of BETA Zeolites. *Chem. Eng. Technol.* **2019**, *42*, 327–342. [[CrossRef](#)]
23. Ahmad, N.N.R.; Leo, C.P.; Mohammad, A.W.; Ahmad, A.L. Modification of gas selective SAPO zeolites using imidazolium ionic liquid to develop polysulfone mixed matrix membrane for CO₂ gas separation. *Microporous Mesoporous Mater.* **2017**, *244*, 21–30. [[CrossRef](#)]
24. Peydayesh, M.; Asarehpour, S.; Mohammadi, T.; Bakhtiari, O. Preparation and characterization of SAPO-34–Matrimid[®] 5218 mixed matrix membranes for CO₂/CH₄ separation. *Chem. Eng. Res. Des.* **2013**, *91*, 1335–1342. [[CrossRef](#)]
25. Zhao, D.; Ren, J.; Li, H.; Hua, K.; Deng, M. Poly (amide-6-b-ethylene oxide)/SAPO-34 mixed matrix membrane for CO₂ separation. *J. Energy Chem.* **2014**, *23*, 227–234. [[CrossRef](#)]
26. Haider, B.; Dilshad, M.R.; Rehman, M.A.U.; Schmitz, J.V.; Kaspereit, M. Highly permeable novel PDMS coated asymmetric polyethersulfone membranes loaded with SAPO-34 zeolite for carbon dioxide separation. *Sep. Purif. Technol.* **2020**, *248*, 116899. [[CrossRef](#)]
27. Mohshim, D.F.; Mukhtar, H.; Man, Z. The effect of incorporating ionic liquid into polyethersulfone-SAPO34 based mixed matrix membrane on CO₂ gas separation performance. *Sep. Purif. Technol.* **2014**, *135*, 252–258. [[CrossRef](#)]
28. Sodeifian, G.; Raji, M.; Asghari, M.; Rezakazemi, M.; Dashti, A. Polyurethane-SAPO-34 mixed matrix membrane for CO₂/CH₄ and CO₂/N₂ separation. *Chin. J. Chem. Eng.* **2019**, *27*, 322–334. [[CrossRef](#)]
29. Junaidi, M.U.M.; Leo, C.P.; Ahmad, A.L.; Kamal, S.N.M.; Chew, T.L. Carbon dioxide separation using asymmetric polysulfone mixed matrix membranes incorporated with SAPO-34 zeolite. *Fuel Process. Technol.* **2014**, *118*, 125–132. [[CrossRef](#)]
30. Rabiee, H.; Alsadat, S.M.; Soltanieh, M.; Mousavi, S.A.; Ghadimi, A. Gas permeation and sorption properties of poly (amide-12-b-ethyleneoxide)(Pebax1074)/SAPO-34 mixed matrix membrane for CO₂/CH₄ and CO₂/N₂ separation. *J. Ind. Eng. Chem.* **2015**, *27*, 223–239. [[CrossRef](#)]
31. Cao, Y.; Kamrani, E.; Mirzaei, S.; Khandakar, A.; Vaferi, B. Electrical efficiency of the photovoltaic/thermal collectors cooled by nanofluids: Machine learning simulation and optimization by evolutionary algorithm. *Energy Rep.* **2022**, *8*, 24–36. [[CrossRef](#)]
32. Li, J.; Xu, K.; Chaudhuri, S. GRASS: Generative recursive autoencoders for shape structures. *ACM Trans. Graph.* **2017**, *36*, 1–14. [[CrossRef](#)]
33. Yeom, C.U.; Kwak, K.C. Performance comparison of ANFIS models by input space partitioning methods. *Symmetry* **2018**, *10*, 700. [[CrossRef](#)]
34. Zamani, H.A.; Rafiee-Taghanaki, S.; Karimi, M.; Arabloo, M.; Dadashi, A. Implementing ANFIS for prediction of reservoir oil solution gas-oil ratio. *J. Nat. Gas Sci. Eng.* **2015**, *25*, 325–334. [[CrossRef](#)]
35. Shojaei, M.J.; Bahrami, E.; Barati, P.; Riahi, S. Adaptive neuro-fuzzy approach for reservoir oil bubble point pressure estimation. *J. Nat. Gas Sci. Eng.* **2014**, *20*, 214–220. [[CrossRef](#)]
36. Shahriari-Kahkeshi, M.; Moghri, M. Prediction of tensile modulus of PA-6 nanocomposites using adaptive neuro-fuzzy inference system learned by the shuffled frog leaping algorithm. *E-Polymers* **2017**, *17*, 187–198. [[CrossRef](#)]
37. Ali, A.; Guo, L. Adaptive neuro-fuzzy approach for prediction of dewpoint pressure for gas condensate reservoirs. *Pet. Sci. Technol.* **2020**, *38*, 673–681. [[CrossRef](#)]
38. Seyed Alizadeh, S.M.; Bagherzadeh, A.; Bahmani, S.; Nikzad, A.; Aminzadehsarikhanbeglou, E.; Tatyana Yu, S. Retrograde gas condensate reservoirs: Reliable estimation of dew point pressure by the hybrid neuro-fuzzy connectionist paradigm. *J. Energy Resour. Technol.* **2021**, *144*, 63007. [[CrossRef](#)]
39. Benmouiza, K.; Chekneane, A. Clustered ANFIS network using fuzzy c-means, subtractive clustering, and grid partitioning for hourly solar radiation forecasting. *Theor. Appl. Climatol.* **2019**, *137*, 31–43. [[CrossRef](#)]

40. Tian, J.; Liu, Y.; Zheng, W.; Yin, L. Smog prediction based on the deep belief-BP neural network model (DBN-BP). *Urban Clim.* **2022**, *41*, 101078. [[CrossRef](#)]
41. Lu, H.; Zhu, Y.; Yin, M.; Yin, G.; Xie, L. Multimodal Fusion Convolutional Neural Network With Cross-Attention Mechanism for Internal Defect Detection of Magnetic Tile. *IEEE Access* **2022**, *10*, 60876–60886. [[CrossRef](#)]
42. Shang, K.; Chen, Z.; Liu, Z.; Song, L.; Zheng, W.; Yang, B.; Liu, S.; Yin, L. Haze prediction model using deep recurrent neural network. *Atmosphere* **2021**, *12*, 1625. [[CrossRef](#)]
43. Xie, L.; Zhu, Y.; Yin, M.; Wang, Z.; Ou, D.; Zheng, H.; Liu, H.; Yin, G. Self-feature-based point cloud registration method with a novel convolutional Siamese point net for optical measurement of blade profile. *Mech. Syst. Signal Process.* **2022**, *178*, 109243. [[CrossRef](#)]
44. Yin, L.; Wang, L.; Zheng, W.; Ge, L.; Tian, J.; Liu, Y.; Yang, B.; Liu, S. Evaluation of empirical atmospheric models using Swarm-C satellite data. *Atmosphere* **2022**, *13*, 294. [[CrossRef](#)]
45. Hosseini, S.; Vaferi, B. Determination of methanol loss due to vaporization in gas hydrate inhibition process using intelligent connectionist paradigms. *Arab. J. Sci. Eng.* **2022**, *47*, 5811–5819. [[CrossRef](#)]